

Analysis of notch effect in the fracture behaviour of 3D printed PLA and 3D printed graphene reinforced PLA

Víctor Martínez-Mata^{1,*}, Sergio Cicero^{1,*}, Laura Castañón-Jano², Alejandro Alonso-Estébanez², Borja Arroyo¹

- ^{1.} LADICIM (Laboratory of Materials Science and Engineering), University of Cantabria, E.T.S. de Ingenieros de Caminos, Canales y Puertos, Av/ Los Castros 44, Santander, 39005 Cantabria, Spain; victor.martinez@unican.es (V.M-M); ciceros@unican.es (S.C); borja.arroyo@unican.es (B.A.)
 - ^{2.} Department of Transport, Projects and Process Technology, University of Cantabria, 39005 Santander, Spain; alejandro.alonso@unican.es (A.A.-E.); laura.castanon@unican.es (L.C.-J.)
- * Corresponding author: ciceros@unican.es

Abstract: The fracture assessment of 3D printed PLA and 3D printed graphene reinforced PLA (PLA-GR) has been performed in this paper. Tensile and fracture specimens were fabricated with three different raster orientations (0/90, 30/-60 and 45/-45) in order to analyse the effect of the printing strategy on the resulting mechanical properties. A total of 30 tensile tests and 120 fracture tests were performed, covering fracture samples with defects of different notch radii (0mm, 0.25mm, 0.5mm, 1mm and 2mm). The Theory of Critical Distances was applied over the fracture results, obtaining estimations of the corresponding critical distances and the subsequent predictions of the apparent fracture toughness. Graphene addition has a different effect depending on the raster orientation. Graphene causes a significant improvement of tensile and fracture properties for specimens fabricated at 30/-60 and 45/-45. However, this phenomenon is not observed in raster orientation 0/90. SEM analysis shows a clear change in the fracture micromechanisms between PLA and PLA-GR. It can be also observed how graphene samples of 30/-60 and 45/-45 present a similar aspect of the fracture surfaces, which are different from those observed in raster orientation 0/90.

1. Introduction

Additive manufacturing is a widely used technology nowadays that allows complex geometries to be fabricated easily. Different manufacturing processes coexist in this technology, such as material extrusion, material jetting, power bed fusion, binder jetting, vat photopolymerization, sheet lamination and directed energy deposition, fused deposition modelling (material extrusion) being the most used. This process consists of passing a wire material through a nozzle, reducing its diameter and depositing it on the printer bed layer by layer. The full process is guided by software that monitors the printing [1].

A number of materials can be printed with this technology, including polymers, metals and composites. When dealing with polymers and polymer-matrix composites, acrylonitrile butadiene styrene (ABS) and polylactic acid (PLA) are the most common materials in this field. PLA ((C₃H₄O₂)_n) will be the base material analysed in this work. It is a biodegradable and sustainable polymer, since it is basically produced from corn, and its main applications cover from biomedical [2] uses to packaging.

The printing process of a given component involves the definition of different printing parameters, many of them having a direct effect on the final mechanical behaviour [3-6]:

layer thickness, raster orientation, infill level, extrusion temperature or feed rate, etc. As an example, the orientation angle of the printing process (raster orientation) is analysed in several works (e.g., [7-9]), where it is observed that tensile properties (yield stress, ultimate tensile stress or Young's modulus) present lower values as the raster orientation gets closer to the perpendicular direction of the applied force. As the material becomes less resistant, it may develop higher strains at failure.

In addition, polymers are commonly combined with other elements in order to improve their properties. Polymer-matrix composites are the result of combining a polymer (the matrix) with another material (or materials) acting as the reinforcement. Graphene and its derivatives (e.g., graphene oxide), have been widely employed as a reinforcing material over the last decade, given that they present outstanding mechanical properties that can significantly improve the mechanical performance of the matrix. The analysis of the mechanical behaviour of composites reinforced with graphene, including 3D-printed materials, has focused mainly on the tensile properties (e.g., [10-13]).

In this context, there is a lack of knowledge about the fracture behaviour of 3D printed materials, especially of polymer-matrix reinforced materials. The presence of printing defects has a direct effect on the material fracture toughness, and the geometry of the defect is decisive in the fracture process. Most of the previous research has analysed specimens containing crack-like defects, not covering the fracture behaviour in the presence of notch-type defects and the corresponding notch effect. This effect may imply a significant increase in the fracture resistance in some materials [14-16], this increase being less evident in other cases [10-12]. For this reason, this paper will be focused on the fracture behaviour of 3D printed PLA and 3D printed PLA reinforced with graphene (PLA-GR), in the presence of U-notches. Different notch radii will be analysed: 0 mm (crack-like defects), 0.25 mm, 0.5 mm, 1 mm and 2 mm. At the same time, different raster orientations will be studied (0/90, 30/-60 and 45/-45), in order to determine how the printing angle affects the observed fracture resistance.

The analysis of the notch effect will be based on the Theory of Critical Distances (TCD), a set of methodologies extensively applied in the last few years, characterised by the use of a material length parameter (the critical distance, L). This theoretical framework will be detailed on Section 2, together with the experimental program. Section 3 gathers the results obtained, and Section 4 presents the main conclusions.

2. Materials and methods

The goal of this research is to analyse the fracture behaviour of both 3D-printed PLA and 3D printed PLA-GR containing U-notches, also evaluating the consequences of including the graphene reinforcement on the final mechanical properties. PLA and PLA-GR filaments were supplied by FiloAlfa3D (Milano, Italy). The content of graphene of the PLA-GR analysed here is fixed at 1 wt.%.

An experimental programme has been carried out in order to characterise the two materials (PLA and PLA-GR). It was composed of 120 fracture tests and 30 tensile tests. Half of the tests were performed on PLA specimens, and the other half on PLA-GR specimens. Moreover, the fracture specimens combined three different raster orientations (0/90, 30/-60 and 45/-45), as is also the case for the tensile specimens, and five different notch radii (0 mm, 0.25 mm, 0.5 mm, 1 mm and 2 mm). Consequently, three tensile tests were performed per raster orientation and four fracture tests were completed per notch

radius (ρ) and raster orientation. A schematic of the specimens, tensile and fracture, is shown in Figure 1.

The specimens used in the fracture tests were Single Edge Notched Bend (SENB) type and their defects were machined, excluding the 0 mm radius defects (crack-like), which were generated by sawing a razor blade following ASTM D6068 [13]. All samples were manufactured by fused deposition modelling (FDM) using a Prusa i3 printer with the following printing parameters: nozzle diameter 0.4 mm; nozzle temperature 200 °C; bed temperature 75 °C; printing rate 30mm/s; infill level 100%; layer height 0.3 mm. As mentioned above, three raster orientations were fabricated, all of them being represented in Figure 2.

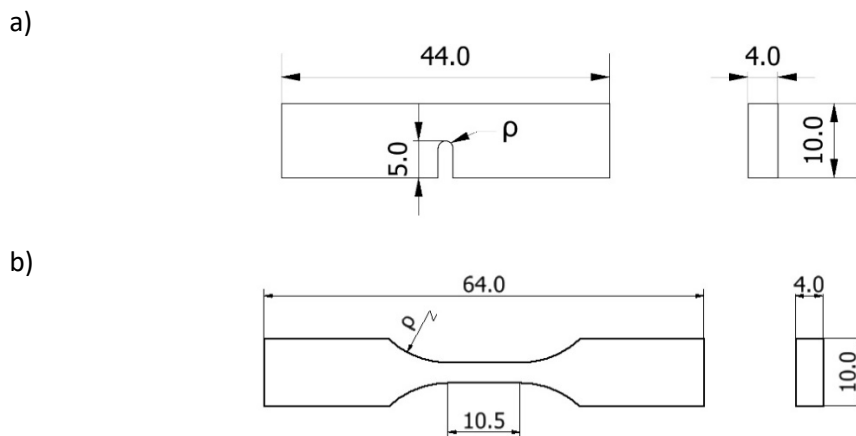


Figure 1: Schematic of the specimens used in the experimental programme: (a) fracture samples; (b) tensile samples. Dimensions in mm.

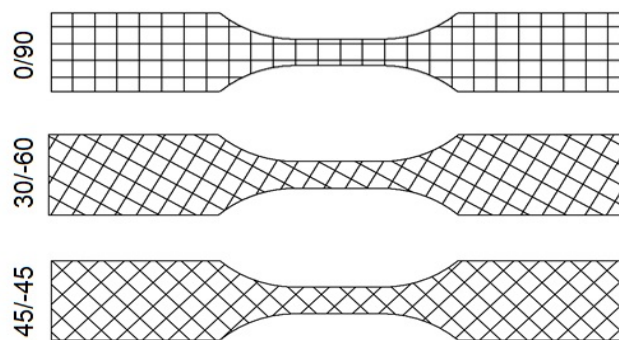


Figure 2: Tensile specimens with the three different raster orientations

A servo-hydraulic testing machine (Servosis, Madrid, Spain) with load capacity of 5 kN was used for the tensile tests. Strain measurements were derived from an axial extensometer (INSTRON, Norwood, MA, USA). The loading rate was 1 mm/min and the tests were performed at room temperature following ASTM638[14].

For the fracture tests an electro-mechanical machine with a load capacity of 2.5kN was employed (Zwick-Roell BT1-FR2.ST5, Zwick-Roell, Ulm, Germany), applying a crosshead displacement rate of 1 mm/min during the tests. The procedure carried out followed ASTM

D6068[13][due to the expected non-linear behaviour. However, other works found in the literature (e.g.,[15]) have reported linear behaviour, something that may be caused by the different printing parameters used in the fabrication of the specimens [16].

The experimental program will be complemented with the application of the TCD, in order to quantify the resulting notch effect through the determination of the apparent fracture toughness (K_{mat}^N) of the notched specimens. This parameter refers to the resistance developed by the material in the presence of a notch, unlike the material fracture toughness (K_{mat}), which is applied when the material contains crack-like defects. Here, a notch is a defect with a radius on the tip different to zero. The TDC comprises different methodologies, all of them characterised by the use of a material length parameter denominated the critical distance (L). The origins of this theory are to be found in the middle of the twentieth century, with the works of Peterson [17] and Neuber [18] . However, the application of the TDC has been widely established and validated in the last two decades (e.g., [14,15,19,20]). The a abovementioned length parameter is usually referred to as L, and in fracture analyses follows equation (1):

$$L = \frac{1}{\pi} \left(\frac{K_{mat}}{\sigma_0} \right)^2 \quad (1)$$

where K_{mat} is the fracture toughness and σ_0 is the material inherent strength. The value of the inherent strength (σ_0) coincides with the material ultimate tensile strength (σ_u) with linear-elastic behaviour at both the micro and the macro scales, whereas in materials with non-linear behaviour σ_0 requires calibration.

The TDC comprises different methodologies [20], but only two of them will be applied in this paper: the point method and the line method. Both of them are based on the stress field at the defect tip being analysed:

- Point method (PM): This is the simplest methodology, and assumes that fracture occurs when the stress reaches the inherent stress, at a distance of r_c from the defect tip. It is proved that the distance (r_c) is equal to L/2 in linear-elastic conditions [24]. The failure criterion is, therefore:

$$\sigma \left(\frac{L}{2} \right) = \sigma_0 \quad (2)$$

- Line method (LM): This methodology establishes that fracture takes place when the average stress along a certain distance reaches the inherent strength (σ_0). The distance is measured from the defect tip, and it is easily demonstrated that it is equal to 2L [24]. The LM expression is:

$$\frac{1}{2L} \int_0^{2L} \sigma(r) dr = \sigma_0 \quad (3)$$

One of the advantages of the TDC is that it allows notched components to be analysed in a relatively simple way: if the fracture in a cracked component occurs when the stress intensity factor (K_I) reaches the material fracture toughness (K_{mat}), the TDC provides a similar assessment, substituting the fracture toughness of the material by the apparent fracture toughness for a notched specimen (K_{mat}^N). Thus, fracture occurs when:

$$K_I = K_{mat}^N \quad (4)$$

The apparent fracture toughness of the notched component (K_{mat}^N) can be estimated from the combination of the Creager-Paris stress field at the notch tip[21] with the different TCD fracture criteria. The expressions, for the PM and LM, are the following:

$$K_{mat}^N = K_{mat} \frac{\left(1 + \frac{\rho}{L}\right)^{3/2}}{\left(1 + \frac{2\rho}{L}\right)} \quad (5)$$

$$K_{mat}^N = K_{mat} \sqrt{1 + \frac{\rho}{4L}} \quad (6)$$

Both expressions will be used below to analyse the notch effect.

Finally, the research programme concludes with a Scanning Electron Microscopy (SEM) analysis of the fracture surfaces, in order to determine the fracture micromechanisms in the different material conditions.

3. Results

3.1. Tensile and fracture results

The main results obtained from the tensile tests (average values and standard deviations) are gathered in Table 1, while some of the tensile curves can be observed in Figure 2. The effect of the graphene is evident, producing an increase in the Young's modulus in all orientations and, simultaneously, a reduction in the material ductility. The samples manufactured at 0/90 show an increase of approximately 10% in the Young's modulus when the graphene is present, and a reduction of 17% in the ductility. The specimens with a raster orientation of 45/-45 show the highest sensitivity to the presence of graphene, obtaining an improvement of 44% in the elasticity modulus, and a reduction of 42% in the ductility. Finally, 30/-60 exhibits intermediate results with an increase of 22% in the Young's modulus, and a 16% decrease in ductility.

At the same time, the raster orientation effect is also shown. Samples manufactured at 0/90 present the highest resistance values with the lowest strains at failure. For the PLA material, as the raster orientation tends to 45°, the material is able to develop higher strains and reduces its rigidity (lower values of Young modulus, yield stress and ultimate tensile strength). The inclusion of graphene reduces the sensibility to raster orientation, and both the resistance and ductility properties are much more similar for the different orientation alternatives.

These observations are also evident in Figure 2. The graphene addition moves the original curves of PLA to the left and upwards, reducing the strain at rupture and, in general, raising the ultimate tensile strength. The raster orientation has the opposite effect on the tensile curves, causing a displacement of the curves to the right and downwards when moving from 0/90 to 45/-45. In any case, the results obtained here are, in general, in accordance with those found in the literature ([22,23]).

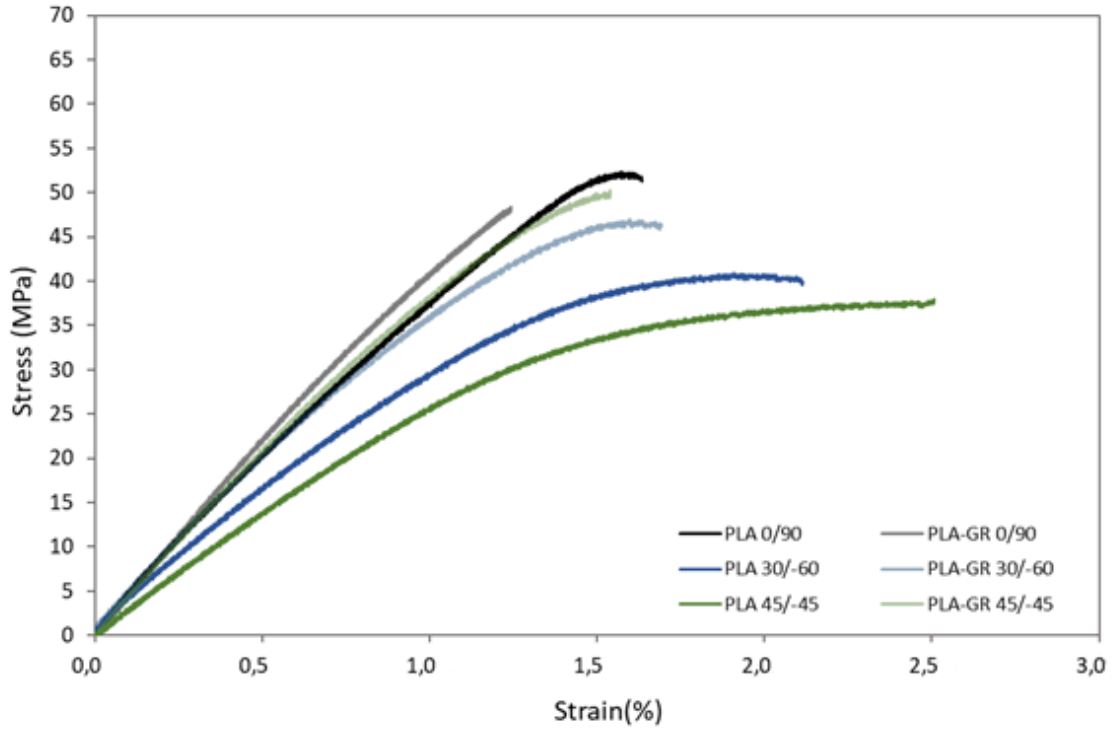


Figure 3: Tensile curves, PLA and PLA-GR, for each raster orientation.

The main results of the fracture tests are shown in Table 2, with the individual results of each tested specimen being gathered in Appendix A. The values of K_{mat}^N have been obtained following ASTM6068 [13], thus, using the same formulation as that used for cracked specimens. Firstly, J_{mat}^N was calculated following equation (7):

$$J_{mat}^N = \frac{\eta \cdot U^N}{B \cdot (W - a_0)} \quad (7)$$

U^N being the area below the load-displacements curve, η being a coefficient equal to 2 in SENB specimens, B being the thickness of the specimen, W being the width of the specimen, and a_0 being the initial defect length. The length of the crack-like defects is the average obtained from three measurements at distances of B/4, B/2 and 3B/4, as per ASTM6068 [20].

Once J_{mat}^N is calculated, K_{mat}^N is derived from equation (8):

$$K_{mat}^N = \sqrt{\frac{J_{mat}^N \cdot E}{1 - \nu^2}} \quad (8)$$

where ν is the Poisson's ratio and E is the Young's modulus.

Figure 4 shows some of the load-displacement curves obtained in the fracture tests for the raster orientation of 45/-45. More specifically, PLA and PLA-GR specimens, with a notch radii of 0 mm and 1 mm, are included. It can be observed how the addition of graphene improves the load-bearing capacity of the material, revealing a clear notch effect. The changes caused by the graphene addition is confirmed in Figure 5, where the notch radius is fixed at 1 mm and the different raster orientations are represented.

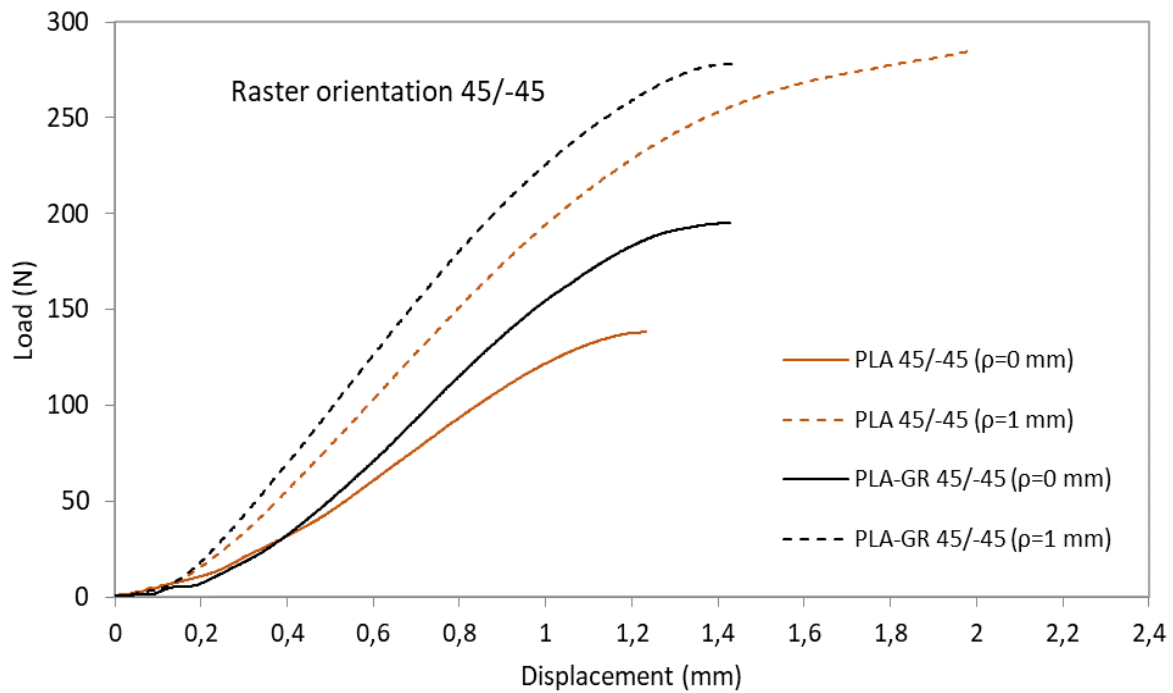


Figure 4: Notch and graphene addition effect for raster orientation 45/-45.

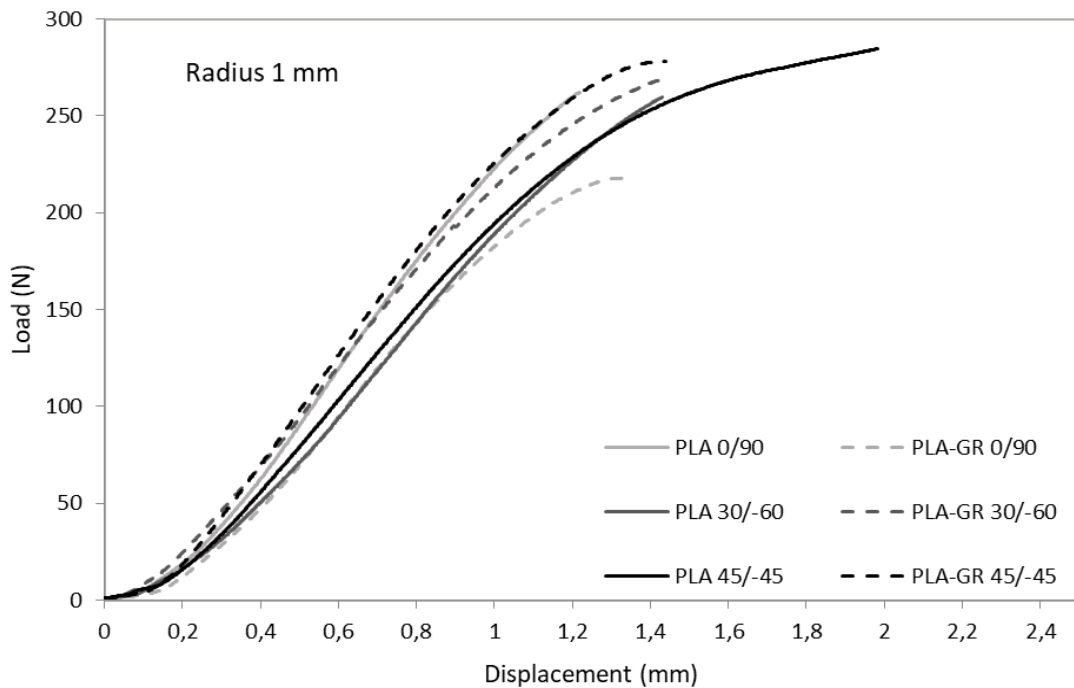


Figure 5. Effect of raster orientation and graphene addition for a fixed notch radius (1 mm).

The presence of graphene has different effects depending on the raster orientation. In the case of 45/-45 specimens, the material becomes more rigid, the displacement at failure decreases and the load-bearing capacity does not change significantly. In the case of the 30/-60 orientation, the material also becomes more rigid, but in this case the displacement at failure remains rather constant and the load-bearing capacity slightly

increases. Finally, the 0/90 orientation presents a different behaviour: the addition of graphene reduces the stiffness and the load-bearing capacity, with the displacement at failure remaining rather constant.

Figures 6, 7 and 8 show the apparent fracture toughness results as a function of the notch radius. In all cases, a clear notch behaviour is observed, given that the apparent fracture toughness generally increases with the notch radius. It is also observed that the notch effect generally saturates at a notch radius of 1 mm, in such a way that a further increase of the notch radius produces a reduction in the apparent fracture toughness (e.g., [7,10]).

In the PLA material, the 0/90 raster orientation presents the higher values of fracture resistance for low notch radii, but its notch effect is more moderate and, thus, its fracture resistance is lower than that observed in the 30/-60 and 45/-45 orientations for the larger radii. This has practical implications when using this type of materials without any graphene addition. Moreover, samples fabricated with an orientation of 0/90 (see Figure 6) present very similar values of apparent fracture toughness for both PLA and PLA-GR, the average difference being less than 10%, and with the PLA material developing slightly higher values.

The 30/-60 and 45/-45 samples (Figures 7 and 8, respectively) present a similar fracture behaviour, with clear differences with that observed in the 0/90 specimens. The addition of graphene increases the apparent fracture toughness by 13% and 19% respectively (average values). This adds another practical implication: when adding graphene, the 0/90 raster orientation should be avoided (as there is no improvement in the fracture behaviour), and 3D printing should be done in different orientations, such as 30/-60 or 45/-45, where significant improvements in the fracture behaviour have been observed. At the same time, the improvement is more pronounced in cracked conditions and becomes more moderate when the notch radius increases, this observation being more evident in the 45/-45 material. The most significant variation is thus observed in cracked specimens of the 45/-45 material (see Figure 10), where the PLA samples present an average fracture toughness value of $4.59 \text{ MPa}\cdot\text{m}^{1/2}$ and the PLA-GR samples develop an apparent fracture toughness of $7.20 \text{ MPa}\cdot\text{m}^{1/2}$. This macroscopic observation will be justified below when observing the corresponding fracture micromechanisms (section 3.3).

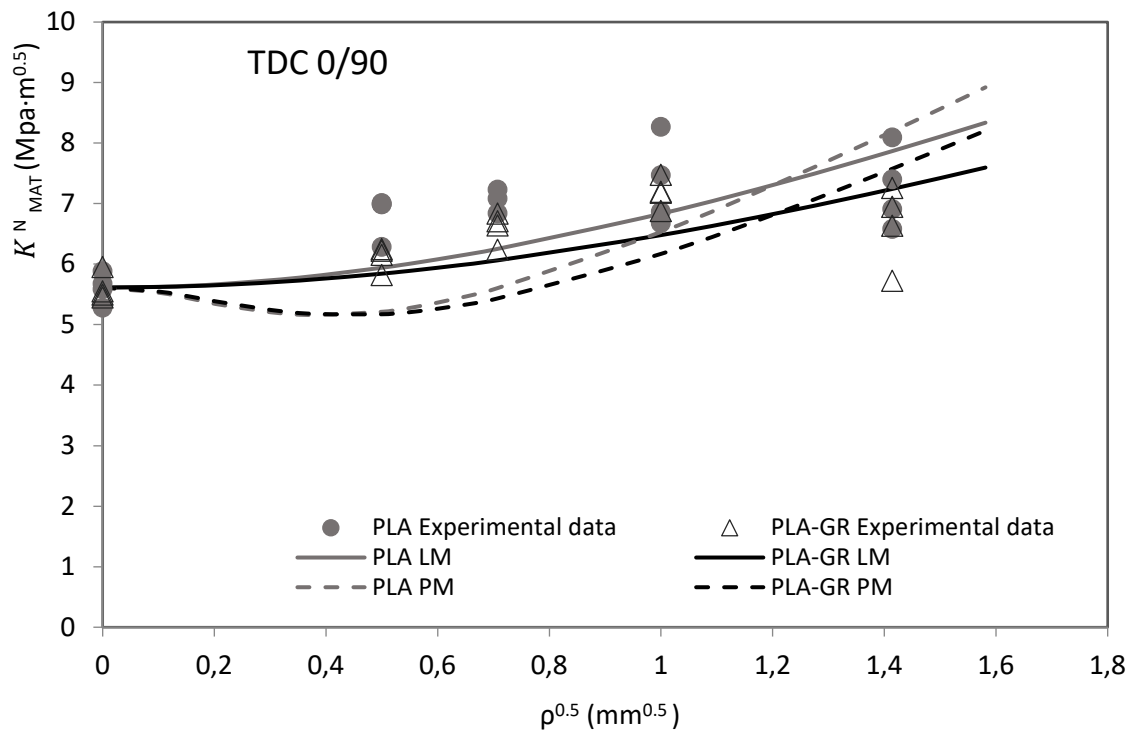


Figure 6: PLA and PLA-GR 0/90 experimental results of apparent fracture toughness and best fit curves when using the LM and the PM.

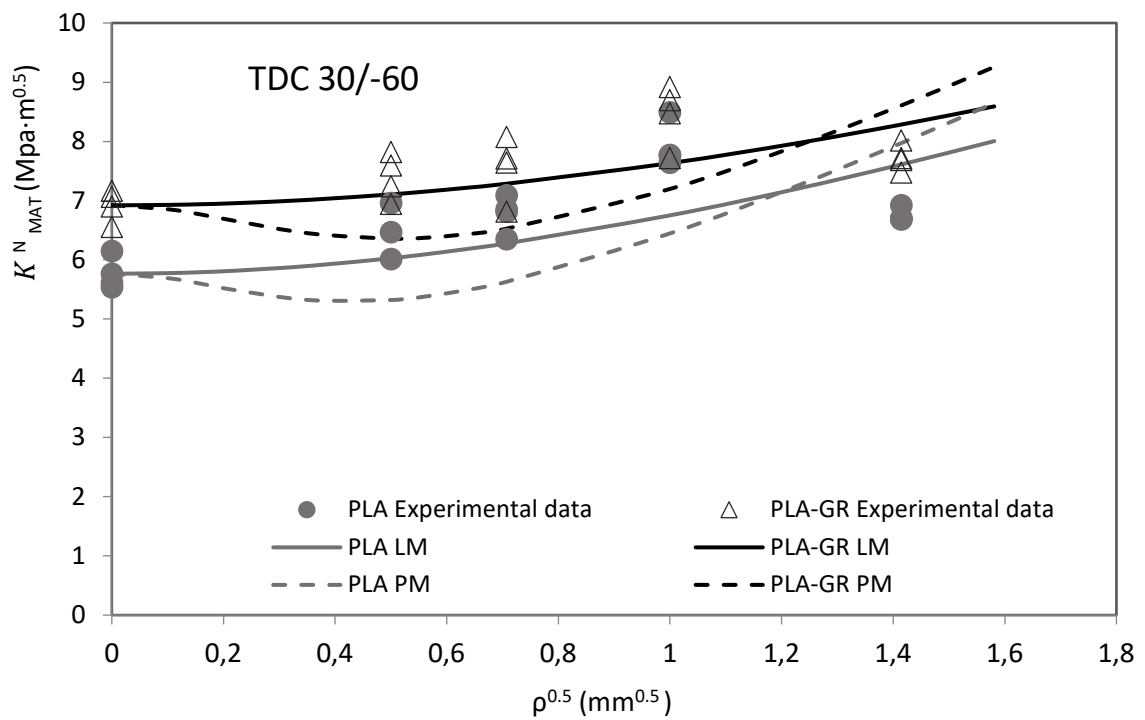


Figure 7: PLA and PLA-GR 30/-60 experimental results of apparent fracture toughness and best fit curves when using the LM and the PM.

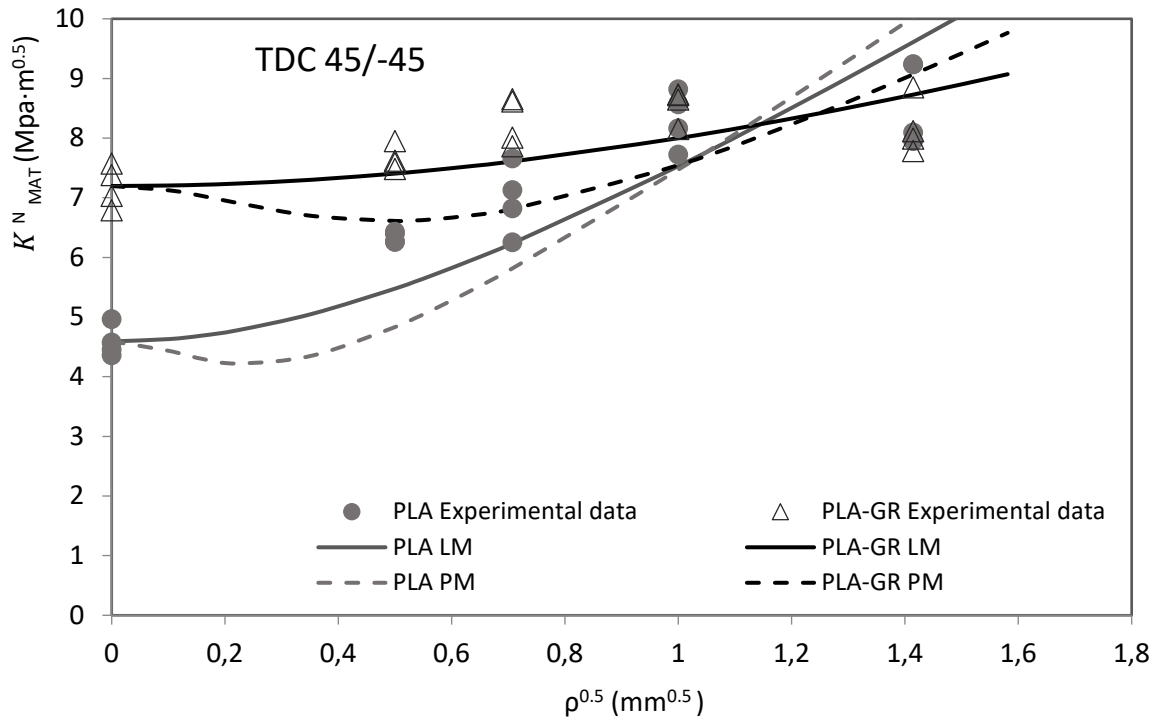


Figure 8: PLA and PLA-GR 45/-45 experimental results of apparent fracture toughness and best fit curves when using the LM and the PM.

3.2. Application of the TCD.

The TCD, briefly outlined above, has been applied in order to derive the critical distance of the PLA and PLA-GR materials. Specifically, the Point Method and the Line Method equations (equations (2) and (3), respectively) have been used to determine this parameter by applying the least squares methodology, with the critical distance (L) being the fitting parameter. The best fitting curves are shown in figures 6 to 8, and the resulting values of L are shown in Table 3. This table also gathers the theoretical L , which is that one derived from equation (1) and assuming purely linear-elastic conditions at fracture (i.e., the inherent strength is set equal to the material ultimate tensile strength, taken from Table 1).

Table 1: Critical distances values (L) derived from the Line Method, the Point Method and the linear-elastic formulation.

	LM	PM	Theoretical L
PLA 0/90	0,52	0,31	3,82
PLA-GR 0/90	0,67	0,39	3,92
PLA 30/-60	0,67	0,36	7,33
PLA-GR 30/-60	1,15	0,50	9,05
PLA 45/-45	0,15	0,12	5,39
PLA-GR 45/-45	1,06	0,48	7,28

The results derived from the LM and the PM are clearly lower than those obtained from the theoretical expression, indicating the presence of non-linear phenomena during

the fracture process. This is more evident in the 45/-45 and 30/-60 orientations, and less pronounced in the 0/90 orientation, in agreement with the load-displacement curves shown above (Figure 5): all the curves are clearly non-linear, with the non-linear behaviour being more noticeable in the 45/-45 and 30/-60 orientations.

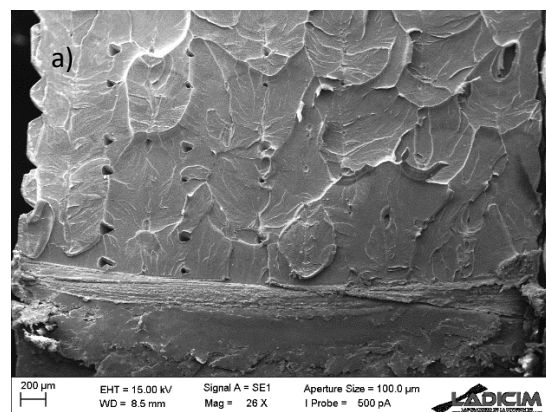
The fitting curves in figure 6 to 8 also reveal that the LM provides better fitting curves for these materials than those provided by the PM.

3.3 SEM analysis

SEM (Scanning Electron Microscopy) analysis has been performed in order to analyse the fracture surface of the different samples (see figures 9 to 11). All specimens present macro-porosity which is usual in 3D printing, even for a 100% infill level.

The PLA samples shows clear brittle micromechanisms, and the addition of graphene causes a significant increase in the rugosity of the fracture surface. This was observed in all raster orientations and can be checked by comparing figures 9a and 9b, 10a and 10b, and 11a and 11b, which correspond to cracked specimens and raster orientations of 0/90, 30/-60 and 45/-45, respectively. Thus, the variation observed between fracture resistance in PLA and PLA-GR specimens may be justified by the modification of the fracture micromechanisms. However, it is important to notice that the fracture resistance of the 0/90 orientation does not improve when adding graphene (see above), in spite of the changes observed in the fracture surface. The reason is that for this very particular raster orientation (see figure 9b), the change in fracture micromechanisms is only observed in the filaments oriented in the perpendicular direction to the acting stresses (90° orientation), whereas the filaments oriented in the same direction as the acting stresses (0° orientation) remain brittle. This is not the case of raster orientations 30/-60 and 45/-45 (see figures 10b and 11b, respectively), in which all the filaments change the fracture micromechanisms when adding graphene, thus providing a significant impact on the fracture behaviour.

The two materials, with the different raster orientations, present a clear notch effect. This is also accompanied by a change in fracture micromechanisms. As an example, Figure 9c represents a PLA specimen with a 2.0 mm notch radius. By comparison with the cracked specimens (Figure 9a), there is a clear change in the fracture surface, which becomes flatter and more homogeneous. Analogous observations were made in raster orientations 30/-60 and 45/-45 when comparing cracked and notched specimens, and are also in agreement with the evolution in fracture micromechanisms observed in other materials when introducing notch radii (e.g., [14-18]).



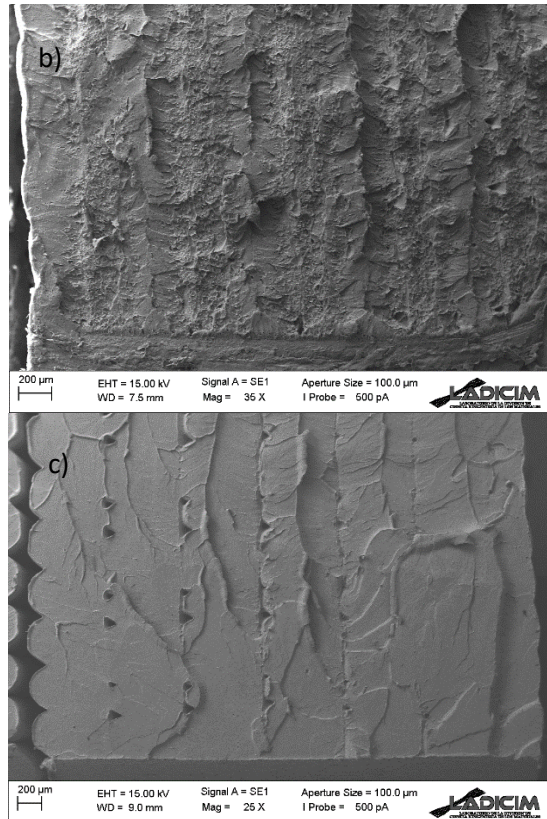
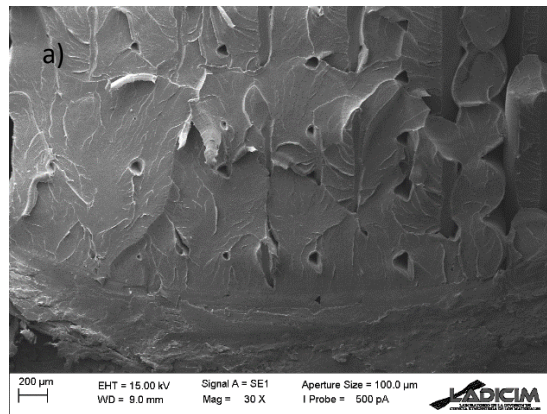


Figure 9 : SEM images obtained from 0/90 raster orientation; (a) general view of PLA cracked sample; (b) overall view of PLA-GR specimen. (c) PLA specimen with a notch radius of 2mm.



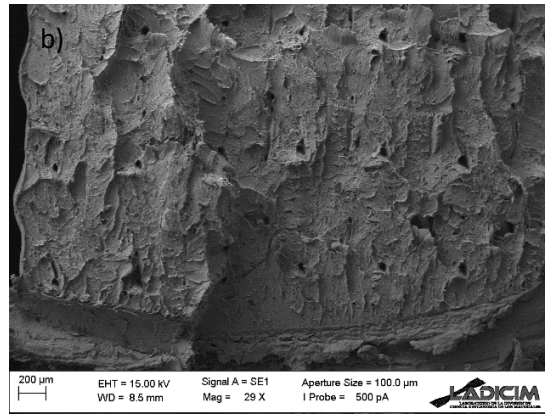


Figure 10: SEM images obtained from 30/-60 raster orientation; (a) general view of PLA cracked sample; (b) overall view of PLA-GR specimen.

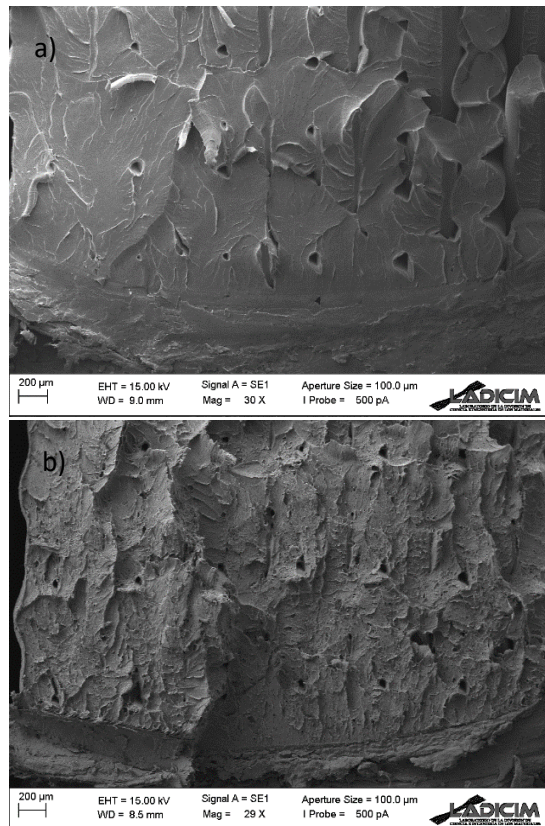


Figure 11: SEM images obtained from raster orientation 45/-45. (a) general view of PLA cracked sample; (b) overall view of PLA-GR specimen.

4. Conclusions

This paper analyses the fracture behaviour and the notch effect observed in 3D printed PLA and 3D printed PLA with graphene (PLA-GR) specimens with different raster orientations: 0/90, 30/-60 and 45/-45. The U-notches covered in the work have notch radii ranging from 0 mm up to 2 mm. The experimental programme was composed of tensile and fracture tests, and the analysis was completed by the application of the Theory of Critical Distances (TDC) and SEM observations of the fracture surfaces. The main conclusions are the following:

- Concerning the tensile behaviour, the addition of graphene rigidizes the materials, increasing the Young's modulus, and reduces the strain at rupture. The effect on the ultimate tensile strength depends on the raster orientation: it is slightly reduced in the 0/90 orientation, slightly increased in 30/-60 and significantly increased in 45/-45.
- Concerning the fracture behaviour, both PLA and PLA-GR develop a clear notch effect.
- In pure PLA and in the presence of crack-like defects, 0/90 raster orientation provides better fracture resistance, but if notch-type defects are expected, 30/-60 and 45/-45 have greater fracture resistance.
- When adding graphene, the 0/90 raster orientation provides the lowest values of apparent fracture toughness regardless of the notch radius.
- The addition of graphene generates evident apparent fracture toughness improvements in the 30/-60 and 45/-45 raster orientations. On the contrary, raster orientation 0/90 does not show any enhancement in the fracture behaviour when adding graphene.
- The TCD may be used, after a calibration process, to provide estimations of the apparent fracture toughness in these materials. The curves generated by the Line Method fit the experimental results better than the curves generated by the Point Method.
- The SEM analysis has justified the evolution of the fracture resistance when adding graphene to the PLA material, as well as the notch effect observed in the different materials and raster orientations.

Acknowledgments

The authors of this work would like to express their gratitude to the Spanish Ministry of Science and Innovation for the financial support of the project PGC2018-095400-B-I00 "Comportamiento en fractura de materiales compuestos nano-reforzados con defectos tipo entalla".

Appendix A

Table A1: Individual test results in PLA and PLA-GR for raster orientation 0/90.

Material	Raster Orientation	Test	Notch Radius, ρ (mm)	W (mm)	b (mm)	a_0 (mm)	K_{mat}^N (MPa·m ^{1/2})	K_{mat}^N avg. (MPa·m ^{1/2})
PLA	0/90	1	0,00	11,05	4,00	5,19	5,59	
PLA	0/90	2	0,00	11,02	4,00	5,05	5,28	5,61
PLA	0/90	3	0,00	11,12	4,00	5,15	5,89	
PLA	0/90	4	0,00	11,07	4,00	4,97	5,68	
PLA	0/90	1	0,25	11,00	4,00	5,00	7,01	6,82
PLA	0/90	2	0,25	10,90	4,00	5,00	6,29	
PLA	0/90	3	0,25	11,10	4,00	5,00	6,99	
PLA	0/90	4	0,25	10,85	4,00	5,00	6,99	
PLA	0/90	1	0,50	11,11	4,00	5,00	7,09	7,06
PLA	0/90	2	0,50	11,08	4,00	5,00	6,84	
PLA	0/90	3	0,50	11,11	4,00	5,00	7,24	
PLA	0/90	4	0,50	10,86	4,00	5,00	non-valid	

PLA	0/90	1	1,00	11,08	4,00	5,00	7,47	
PLA	0/90	2	1,00	11,10	4,00	5,00	8,27	7,32
PLA	0/90	3	1,00	10,96	4,00	5,00	6,87	
PLA	0/90	4	1,00	11,09	4,00	5,00	6,68	
PLA	0/90	1	2,00	10,92	4,00	5,00	7,40	
PLA	0/90	2	2,00	11,11	4,00	5,00	6,91	7,25
PLA	0/90	3	2,00	10,93	4,00	5,00	8,10	
PLA	0/90	4	2,00	10,92	4,00	5,00	6,59	
PLA-GR	0/90	1	0,00	10,89	4,00	5,05	5,55	
PLA-GR	0/90	2	0,00	10,90	4,00	5,02	5,45	5,61
PLA-GR	0/90	3	0,00	10,73	4,00	5,29	5,95	
PLA-GR	0/90	4	0,00	10,84	4,00	5,06	5,50	
PLA-GR	0/90	1	0,25	10,85	4,00	5,00	5,82	
PLA-GR	0/90	2	0,25	10,87	4,00	5,00	6,25	6,11
PLA-GR	0/90	3	0,25	10,86	4,00	5,00	6,22	
PLA-GR	0/90	4	0,25	10,94	4,00	5,00	6,15	
PLA-GR	0/90	1	0,50	10,87	4,00	5,00	6,24	
PLA-GR	0/90	2	0,50	10,79	4,00	5,00	6,71	6,61
PLA-GR	0/90	3	0,50	10,92	4,00	5,00	6,84	
PLA-GR	0/90	4	0,50	10,83	4,00	5,00	6,64	
PLA-GR	0/90	1	1,00	10,90	4,00	5,00	7,48	
PLA-GR	0/90	2	1,00	10,95	4,00	5,00	7,20	7,18
PLA-GR	0/90	3	1,00	10,84	4,00	5,00	7,18	
PLA-GR	0/90	4	1,00	10,85	4,00	5,00	6,88	
PLA-GR	0/90	1	2,00	10,76	4,00	5,00	6,64	
PLA-GR	0/90	2	2,00	10,89	4,00	5,00	6,95	6,64
PLA-GR	0/90	3	2,00	10,90	4,00	5,00	7,26	
PLA-GR	0/90	4	2,00	10,89	4,00	5,00	5,73	

Table A2: Individual test results in PLA and PLA-GR for raster orientation 30/-60.

Material	Raster Orientation	Test	Notch Radius, ρ	W	b	a_0	K_{mat}^N	K_{mat}^N avg.
			(mm)	(mm)	(mm)	(mm)	(MPa·m ^{1/2})	(MPa·m ^{1/2})
PLA	30/-60	1	0,00	10,92	4,00	5,42	5,76	
PLA	30/-60	2	0,00	10,89	4,00	5,17	5,54	5,76
PLA	30/-60	3	0,00	10,91	4,00	5,27	5,61	
PLA	30/-60	4	0,00	11,01	4,00	5,06	6,15	
PLA	30/-60	1	0,25	11,03	4,00	5,00	non-valid	
PLA	30/-60	2	0,25	11,02	4,00	5,00	6,01	6,48
PLA	30/-60	3	0,25	10,97	4,00	5,00	6,47	
PLA	30/-60	4	0,25	10,95	4,00	5,00	6,96	
PLA	30/-60	1	0,50	10,97	4,00	5,00	6,85	
PLA	30/-60	2	0,50	10,85	4,00	5,00	7,09	6,78
PLA	30/-60	3	0,50	11,05	4,00	5,00	6,35	
PLA	30/-60	4	0,50	10,93	4,00	5,00	6,81	
PLA	30/-60	1	1,00	10,72	4,00	5,00	8,49	7,92
PLA	30/-60	2	1,00	10,79	4,00	5,00	7,64	
PLA	30/-60	3	1,00	11,06	4,00	5,00	7,76	

PLA	30/-60	4	1,00	10,87	4,00	5,00	7,77	
PLA	30/-60	1	2,00	10,79	4,00	5,00	6,70	
PLA	30/-60	2	2,00	10,88	4,00	5,00	6,92	6,75
PLA	30/-60	3	2,00	10,82	4,00	5,00	6,69	
PLA	30/-60	4	2,00	11,01	4,00	5,00	6,68	
PLA-GR	30/-60	1	0,00	11,02	4,00	5,05	7,06	
PLA-GR	30/-60	2	0,00	11,06	4,00	5,00	7,16	6,92
PLA-GR	30/-60	3	0,00	11,14	4,00	5,51	6,90	
PLA-GR	30/-60	4	0,00	11,00	4,00	5,44	6,55	
PLA-GR	30/-60	1	0,25	11,02	4,00	5,00	6,94	
PLA-GR	30/-60	2	0,25	11,15	4,00	5,00	7,82	7,40
PLA-GR	30/-60	3	0,25	11,12	4,00	5,00	7,59	
PLA-GR	30/-60	4	0,25	11,10	4,00	5,00	7,24	
PLA-GR	30/-60	1	0,50	11,02	4,00	5,00	8,07	
PLA-GR	30/-60	2	0,50	11,00	4,00	5,00	6,81	7,56
PLA-GR	30/-60	3	0,50	10,99	4,00	5,00	7,64	
PLA-GR	30/-60	4	0,50	11,07	4,00	5,00	7,71	
PLA-GR	30/-60	1	1,00	11,13	4,00	5,00	8,47	
PLA-GR	30/-60	2	1,00	11,26	4,00	5,00	8,91	8,45
PLA-GR	30/-60	3	1,00	11,18	4,00	5,00	8,70	
PLA-GR	30/-60	4	1,00	11,03	4,00	5,00	7,72	
PLA-GR	30/-60	1	2,00	11,26	4,00	5,00	7,68	
PLA-GR	30/-60	2	2,00	11,02	4,00	5,00	7,71	7,72
PLA-GR	30/-60	3	2,00	11,11	4,00	5,00	8,01	
PLA-GR	30/-60	4	2,00	10,96	4,00	5,00	7,47	

Table A3: Individual test results in PLA and PLA-GR for raster orientation 45/-45.

Material	Raster Orientation	Test	Notch				K_{mat}^N	K_{mat}^N avg.
			Radius, ρ	W	b	a_0		
			(mm)	(mm)	(mm)	(mm)	(MPa·m ^{1/2})	(MPa·m ^{1/2})
PLA	45/-45	1	0,00	10,92	4,00	5,42	4,97	
PLA	45/-45	2	0,00	10,83	4,00	5,17	4,46	4,59
PLA	45/-45	3	0,00	10,89	4,00	5,27	4,58	
PLA	45/-45	4	0,00	10,92	4,00	5,06	4,36	
PLA	45/-45	1	0,25	10,90	4,00	5,00	6,27	
PLA	45/-45	2	0,25	10,89	4,00	5,00	6,40	6,34
PLA	45/-45	3	0,25	10,96	4,00	5,00	6,43	
PLA	45/-45	4	0,25	10,87	4,00	5,00	6,26	
PLA	45/-45	1	0,50	10,93	4,00	5,00	6,25	
PLA	45/-45	2	0,50	10,91	4,00	5,00	7,66	6,97
PLA	45/-45	3	0,50	10,87	4,00	5,00	6,83	
PLA	45/-45	4	0,50	10,87	4,00	5,00	7,13	
PLA	45/-45	1	1,00	10,85	4,00	5,00	8,16	
PLA	45/-45	2	1,00	10,97	4,00	5,00	8,57	8,32
PLA	45/-45	3	1,00	10,85	4,00	5,00	8,82	
PLA	45/-45	4	1,00	10,83	4,00	5,00	7,73	
PLA	45/-45	1	2,00	10,85	4,00	5,00	8,10	8,63
PLA	45/-45	2	2,00	10,93	4,00	5,00	9,24	

PLA	45/-45	3	2,00	10,85	4,00	5,00	7,95	
PLA	45/-45	4	2,00	10,95	4,00	5,00	9,24	
PLA-GR	45/-45	1	0,00	11,08	4,00	5,05	7,58	
PLA-GR	45/-45	2	0,00	11,09	4,00	5,00	7,38	7,20
PLA-GR	45/-45	3	0,00	11,05	4,00	5,51	7,03	
PLA-GR	45/-45	4	0,00	10,83	4,00	5,44	6,79	
PLA-GR	45/-45	1	0,25	11,00	4,00	5,00	7,95	
PLA-GR	45/-45	2	0,25	10,90	4,00	5,00	7,48	7,66
PLA-GR	45/-45	3	0,25	11,17	4,00	5,00	7,62	
PLA-GR	45/-45	4	0,25	10,85	4,00	5,00	7,58	
PLA-GR	45/-45	1	0,50	11,14	4,00	5,00	8,01	
PLA-GR	45/-45	2	0,50	11,08	4,00	5,00	7,87	8,29
PLA-GR	45/-45	3	0,50	11,13	4,00	5,00	8,65	
PLA-GR	45/-45	4	0,50	10,86	4,00	5,00	8,62	
PLA-GR	45/-45	1	1,00	11,08	4,00	5,00	8,73	
PLA-GR	45/-45	2	1,00	11,10	4,00	5,00	8,15	8,57
PLA-GR	45/-45	3	1,00	10,96	4,00	5,00	8,65	
PLA-GR	45/-45	4	1,00	11,13	4,00	5,00	8,73	
PLA-GR	45/-45	1	2,00	10,92	4,00	5,00	8,12	
PLA-GR	45/-45	2	2,00	11,11	4,00	5,00	7,99	8,19
PLA-GR	45/-45	3	2,00	10,93	4,00	5,00	8,85	
PLA-GR	45/-45	4	2,00	10,93	4,00	5,00	7,78	

References

- [1] Dwiwati ST, Kholil A, Riyadi R, Putra SE. Influence of layer thickness and 3D printing direction on tensile properties of ABS material. *J Phys Conf Ser* 2019;1402. <https://doi.org/10.1088/1742-6596/1402/6/066014>.
- [2] Murariu M, Dubois P. PLA composites: From production to properties. *Adv Drug Deliv Rev* 2016;107:17–46. <https://doi.org/10.1016/j.addr.2016.04.003>.
- [3] Graphene L, Rafiee M a, Rafiee J, Wang Z, Song H, Yu Z, et al. Enhanced Mechanical Properties of. *ACS Nano* 2009;3:3884–90. <https://doi.org/10.1021/nn9010472>.
- [4] Shen MY, Chang TY, Hsieh TH, Li YL, Chiang CL, Yang H, et al. Mechanical properties and tensile fatigue of graphene nanoplatelets reinforced polymer nanocomposites. *J Nanomater* 2013;2013. <https://doi.org/10.1155/2013/565401>.
- [5] Caminero MÁ, Chacón JM, García-Plaza E, Núñez PJ, Reverte JM, Becar JP. Additive manufacturing of PLA-based composites using fused filament fabrication: Effect of graphene nanoplatelet reinforcement on mechanical properties, dimensional accuracy and texture. *Polymers (Basel)* 2019;11. <https://doi.org/10.3390/polym11050799>.
- [6] Marconi S, Alaimo G, Mauri V, Torre M, Auricchio F. Impact of graphene reinforcement on mechanical properties of PLA 3D printed materials. *2017 IEEE MTT-S Int Microw Work Ser Adv Mater Process RF THz Appl IMWS-AMP 2017 2018*;2018-Janua:1–3. <https://doi.org/10.1109/IMWS-AMP.2017.8247414>.
- [7] Cicero S, Madrazo V, Carrascal IA. Analysis of notch effect in PMMA using the Theory of Critical Distances. *Eng Fract Mech* 2012;86:56–72. <https://doi.org/10.1016/j.engfracmech.2012.02.015>.
- [8] Cicero S, Madrazo V, García T. Analysis of notch effect in the apparent fracture

toughness and the fracture micromechanisms of ferritic-pearlitic steels operating within their lower shelf. *Eng Fail Anal* 2014;36:322–42.
<https://doi.org/10.1016/j.engfailanal.2013.10.021>.

- [9] Cicero S, García T, Madrazo V. Application and validation of the notch master curve in medium and high strength structural steels. *J Mech Sci Technol* 2015;29:4129–42.
<https://doi.org/10.1007/s12206-015-0907-2>.
- [10] Cicero S, Martínez-Mata V, Alonso-Estebanez A, Castanon-Jano L, Arroyo B. Analysis of notch effect in 3D-printed ABS fracture specimens containing U-notches. *Materials (Basel)* 2020;13:1–13. <https://doi.org/10.3390/ma13214716>.
- [11] Ibáñez-Gutiérrez FT, Cicero S, Carrascal IA. On the influence of moisture content on the fracture behaviour of notched short glass fibre reinforced polyamide 6. *Compos Part B Eng* 2019;159:62–71. <https://doi.org/10.1016/j.compositesb.2018.09.062>.
- [12] Cicero S, García T, Castro J, Madrazo V, Andrés D. Analysis of notch effect on the fracture behaviour of granite and limestone: An approach from the Theory of Critical Distances. *Eng Geol* 2014;177:1–9. <https://doi.org/10.1016/j.enggeo.2014.05.004>.
- [13] ASTM D6068 “ Standar method for determining J-R cuves of plastic materials” 2014.
- [14] International A. ASTM D638-14, Standard Test Method for Tensile Properties of Plastics. West Conshohocken, PA: ASTM International; 2014.
- [15] Ezeh OH, Susmel L. On the notch fatigue strength of additively manufactured polylactide (PLA). *Int J Fatigue* 2020;136:105583.
<https://doi.org/10.1016/j.ijfatigue.2020.105583>.
- [16] Kiendl J, Gao C. Controlling toughness and strength of FDM 3D-printed PLA components through the raster layup. *Compos Part B Eng* 2020;180:107562.
<https://doi.org/10.1016/j.compositesb.2019.107562>.
- [17] Peterson RE. Notch Sensitivity, Metal Fatigue, G. Sines, J. Lwaisman. New York McGrawHill 1959.
- [18] Neuber H. Theory of notch stresses: principles for exact calculation of strength with reference to structural form and material. Berlin, Germany: Springer Verlag; 1958.
- [19] Justo J, Castro J, Cicero S, Sánchez-Carro MA, Husillos R. Notch effect on the fracture of several rocks: Application of the Theory of Critical Distances. *Theor Appl Fract Mech* 2017;90:251–8. <https://doi.org/10.1016/j.tafmec.2017.05.025>.
- [20] Taylor D. The theory of critical distances: a new perspective in fracture mechanics. London: Elsevier; 2007.
- [21] Creager, Matthew; Paris P. Elastic field equations for blunt cracks with reference to stress corrosion cracking. 1697.
- [22] Chieng BW, Ibrahim NA, Yunus WMZW, Hussein MZ. Poly(lactic acid)/poly(ethylene glycol) polymer nanocomposites: Effects of graphene nanoplatelets. *Polymers (Basel)* 2014;6:93–104. <https://doi.org/10.3390/polym6010093>.
- [23] Ayatollahi MR, Nabavi-Kivi A, Bahrami B, Yazid Yahya M, Khosravani MR. The influence of in-plane raster angle on tensile and fracture strengths of 3D-printed PLA specimens. *Eng Fract Mech* 2020;237:107225.
<https://doi.org/10.1016/j.engfracmech.2020.107225>.

Figure Captions

Figure 12: Schematic of the specimens used in the experimental programme: (a) fracture samples; (b) tensile samples. Dimensions in mm.

Figure 13: Tensile specimens with the three different raster orientations

Figure 14: Tensile curves, PLA and PLA-GR, for each raster orientation.

Figure 15: Notch and graphene addition effect for raster orientation 45/-45.

Figure 16. Effect of raster orientation and graphene addition for a fixed notch radius (1 mm).

Figure 17: PLA and PLA-GR 0/90 experimental results of apparent fracture toughness and best fit curves when using the LM and the PM.

Figure 18: PLA and PLA-GR 30/-60 experimental results of apparent fracture toughness and best fit curves when using the LM and the PM.

Figure 19: PLA and PLA-GR 45/-45 experimental results of apparent fracture toughness and best fit curves when using the LM and the PM.

Figure 20 : SEM images obtained from 0/90 raster orientation; (a) general view of PLA cracked sample; (b) overall view of PLA-GR specimen. (c) PLA specimen with a notch radius of 2mm.

Figure 10: SEM images obtained from 30/-60 raster orientation; (a) general view of PLA cracked sample; (b) overall view of PLA-GR specimen.

Figure 11: SEM images obtained from raster orientation 45/-45. (a) general view of PLA cracked sample; (b) overall view of PLA-GR specimen.

Tables

Table 2: Tensile properties for PLA and PLA-GR in each raster orientation. E: Young's modulus; σ_y : Yield stress; σ_u : ultimate tensile strength; ϵ_u : Strain under maximum load.

Material	Raster orientation	E (MPa)	σ_y (MPa)	σ_u (MPa)	ϵ_u (%)
PLA	0/90	3769 ± 218	51,2 ± 0,9	52,0 ± 0,9	1,7 ± 0,2
PLA-GR	0/90	4135 ± 277	50,5 ± 4,1	51,0 ± 4,4	1,4 ± 0,3
PLA	30/-60	3313 ± 212	38,0 ± 3,7	42,0 ± 3,0	1,9 ± 0,1
PLA-GR	30/-60	4065 ± 362	41,0 ± 2,7	44,3 ± 2,3	1,6 ± 0,2
PLA	45/-45	2751 ± 406	35,3 ± 4,6	41,1 ± 5,7	2,6 ± 0,2
PLA-GR	45/-45	3972 ± 260	47,5 ± 1,4	49,0 ± 2,8	1,5 ± 0,2

Table 3: Fracture results obtained for each raster orientation. K_{mat}^N : apparent fracture toughness.

Material	Notch radius(mm)	0/90	30/-60	45/-45
		K_{mat}^N (Mpa·m ^{0.5})		
PLA	0,00	5,61	5,76	4,59
PLA	0,25	6,82	6,48	6,34
PLA	0,50	7,06	6,78	6,97
PLA	1,00	7,32	7,92	8,32
PLA	2,00	7,25	6,75	8,63
PLA-GR	0,0	5,61	6,92	7,20
PLA-GR	0,25	6,11	7,40	7,66
PLA-GR	0,50	6,61	7,56	8,29
PLA-GR	1,00	7,18	8,45	8,57
PLA-GR	2,00	6,64	7,72	8,19